JACS
JOURNAL OF THE AMERICAN CHEMICAL SOCIETY

pubs.acs.org/JACS

Article

Cell-Penetrating Streptavidin: A General Tool for Bifunctional Delivery with Spatiotemporal Control, Mediated by Transport Systems Such as Adaptive Benzopolysulfane Networks

Javier López-Andarias,* Jacques Saarbach, Dimitri Moreau, Yangyang Cheng, Emmanuel Derivery, Quentin Laurent, Marcos González-Gaitán, Nicolas Winssinger, Naomi Sakai, and Stefan Matile*

Cite This: J. Am. Chem. Soc. 2020, 142, 4784−4792

Read Online

ACCESS | Metrics & More | Article Recommendations | Supporting Information

ABSTRACT: In this report, cell-penetrating streptavidin (CPS) is introduced to exploit the full power of streptavidin−biotin biotechnology in cellular uptake. For this purpose, transporters, here cyclic oligochalcogenides (COCs), are covalently attached to lysines of wild-type streptavidin. This leaves all four biotin binding sites free for at least bifunctional delivery. To maximize the standards of the quantitative evaluation of cytosolic delivery, the recent chloroalkane penetration assay (CAPA) is coupled with automated high content (HC) imaging, a technique that combines the advantages of fluorescence microscopy and flow cytometry. According to the resulting HC-CAPA, cytosolic delivery of CPS equipped with four benzopolysulfanes was the best among all tested CPSs, also better than the much smaller TAT peptide, the original cell-penetrating peptide from HIV. HaloTag-GFP fusion proteins expressed on mitochondria were successfully targeted using CPS carrying two different biotinylated ligands, HaloTag substrates or anti-GFP nanobodies, interfaced with peptide nucleic acids, flipper force probes, or fluorescent substrates. The delivered substrates could be released from CPS into the cytosol through desthiobiotin−biotin exchange. These results validate CPS as a general tool which enables unrestricted use of streptavidin−biotin biotechnology in cellular uptake.

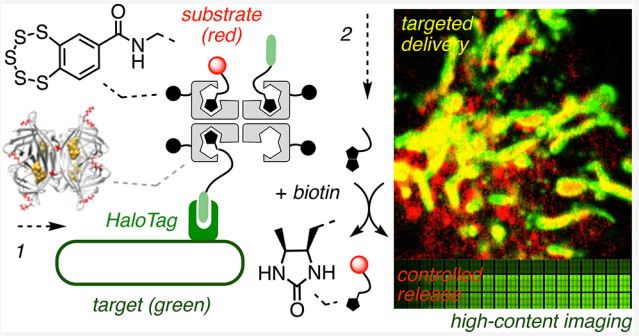

INTRODUCTION

Streptavidin[1−4] is a 52 kDa β-barrel tetramer that binds one biotin per monomer with exceptionally high affinity because the barrels close upon binding (Figure 1A). The advantages of such encapsulation combined with tetravalency, stability, and ease of use empower the high versatility of biotin−streptavidin technology. For cellular uptake, streptavidin has been used to noncovalently couple biotinylated substrates to biotinylated transporters such as cell-penetrating peptides (CPPs)[5] and other dynamic covalent systems,[6] including cell-penetrating poly(disulfide)s,[7,8] related disulfide-containing systems,[9,10] and cyclic oligochalcogenides (COCs, Figure 1B).[11−15] However, this approach is limited to the reliable delivery of only one functionality because it is difficult to control the interfacing of more than two different ligands with the streptavidin tetramer. This limitation is occasionally overcome by covalent linking of fluorophores to proteins.[14] A more powerful solution would be cell-penetrating streptavidin (CPS) with covalently attached transporters and all four binding sites free to harness the full power of streptavidin−biotin technology for bifunctional delivery (Figure 1C) with, for example, retention-using-selective-hooks (RUSH)-like[16] spatiotemporal control (Figure 1D).

Covalent protein modification has been used previously for cellular uptake. Examples include supercharging of proteins by either addition of positive or removal of negative charges[17] or simple covalent conjugation to possible new transporters such as boronic acids or halogen-bond donors.[5−10,18]

To elaborate on the idea of CPS, we selected COCs as transporters. COCs such as asparagusic acid (AA),[11,12] epidiketodithiopiperazines,[13] diselenolipoic acid (DSL),[14] or the most recent benzopolysulfanes (BPS)[15] are currently being explored to access increasingly unorthodox dynamic covalent oligochalcogenide exchange chemistry on the way into the cytosol. Such thiol-mediated uptake of COCs[11−15] and related transporters[7−10] has allowed delivery of not only small molecules but also larger substrates such as DNA,[9b] antibodies,[9c] quantum dots,[8] other nanoparticles,[9c] liposomes, and polymersomes[11d] to the cytosol without significant capture

Received: December 18, 2019
Published: February 28, 2020

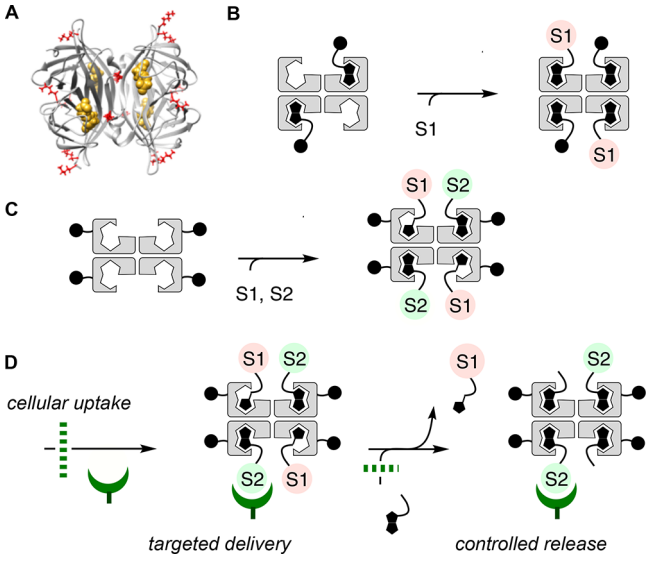

Figure 1. (A) Molecular model of wild-type streptavidin tetramer with bound biotins (yellow) and lysine residues (red, front view) used to (C) covalently attach transporters. (B) Conventional use of streptavidin to interface biotinylated transporters with one biotinylated substrate. (C) Cell-penetrating streptavidin (CPS) with all biotin binding sites free to interface with two different biotinylated substrates S1 and S2 for bifunctional uptake with (D) spatiotemporal control.

within endosomes. Mechanistic hypotheses envision COCs as molecular walkers, walking along disulfide tracks in membrane proteins[12,14,19,20] through the transient micellar pores known from CPPs but also from disulfide-rich scramblases or voltage-gated ion channels (Figures 2B and 2C).[14,20,21] Driving the growing impact of dynamic covalent chemistry to cellular uptake[6−14] to the extreme, BPS have been hypothesized to act by forming adaptive networks of rare sulfur species such as macrocycles **1** containing up to 19 sulfur atoms for cells to select from (Figure 2D).[15] BPS are known to occur in marine natural products,[22] have attracted early attention in total synthesis,[23] and appeared top in recent library screens to reverse cognitive defects in mouse models.[24]

The objective of this study was to create a general tool which warrants unrestricted availability of streptavidin−biotin technology in cellular uptake. With COCs as a timely example of freely variable transporters, bifunctional delivery with spatiotemporal[16] controllability is tackled as a functional challenge of biological relevance (Figure 1D). Specifically, HC-CAPA, a new combination of the chloroalkane penetration assay (CAPA)[25,26] with automated high content fluorescence microscopy,[27] is introduced first to secure direct quantitative functional evidence for cytosolic delivery of CPS. On the basis of these results, compatibility of CPS with targeted delivery, the interfacing of nanobodies,[8] peptide nucleic acids (PNAs),[28] and mechanosensitive fluorescent flipper probes[29] with HaloTag-GFP fusion proteins,[25,30] and their controlled release through intracellular desthiobiotin−biotin exchange are demonstrated.[3,4,16,29a]

RESULTS AND DISCUSSION

Design and Synthesis of CPS. Wild-type streptavidin tetramer **2** contains 16 lysine residues (Figures 1A and 2A),[1−4] which were partially derivatized to give CPS with different numbers of COCs. We chose to chemically modify amines

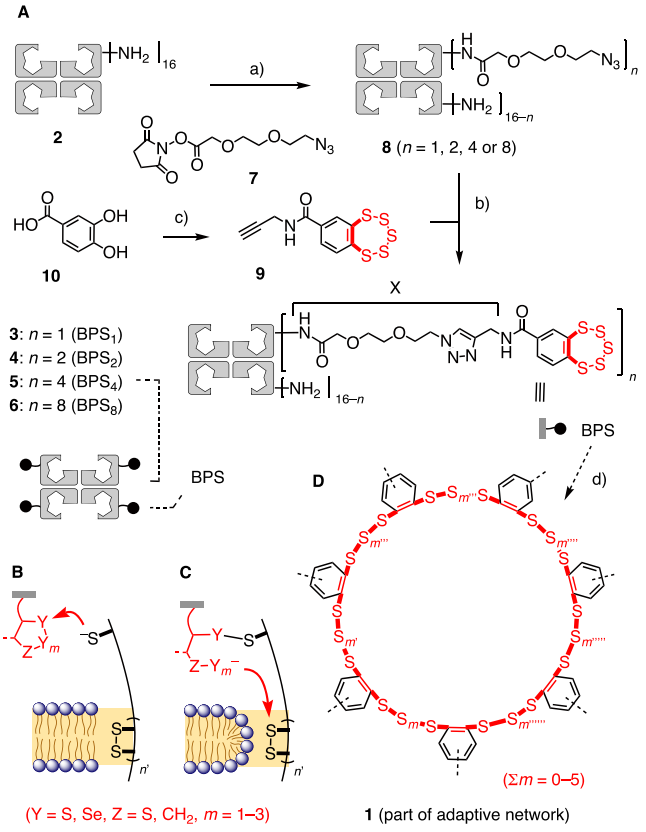

Figure 2. (A) Synthesis of CPSs **3**−**6**: (a) PBS, pH 7.4, rt, 2 h; (b) $CuSO_4 \cdot 5H_2O$, BTTAA, sodium ascorbate, aminoguanidine hydrochloride, PBS, pH 7.4, rt, 1 h; (c, d) ref 15. (B−D) Working hypotheses for the modes of action of COCs as molecular walkers (B) first exchanging with exofacial thiols and (C) then walking along disulfide tracks and transient micellar pores into cells and of (D) BPS as an adaptive network including macrocycles as large as **1**.

rather than carboxylates to preclude misleading CPP-like contributions[5−8,21] to the uptake activity of CPS due to increased net positive charge.[26,17] The synthesis of CPSs **3**−**6** is shown as an example (Figures 2A and 3, Schemes S7 and S8). The reaction of **2** and a controlled amount of activated ester **7** gave modified streptavidin **8** with up to ca. eight azide groups. The degree of functionalization was estimated using a colorimetric amine assay (Figure S1). The obtained key intermediate **8** underwent copper-catalyzed alkyne−azide cycloaddition reaction (CuAAC) quantitatively with alkynylated transporter **9** under mild conditions to give CPSs with ca. one (**3**, BPS_1), two (**4**, BPS_2), four (**5**, BPS_4) or eight covalently linked BPSs (**6**, BPS_8, Figure 2A). BPS **9** was prepared by multistep synthesis from catechol **10** following previously reported procedures.[15] CuAAC between pre-CPS **8** and other alkynylated transporters and controls afforded CPSs covalently linked with four or eight AAs (**11**, AA_4; **12**, AA_8), four AA-arginines (**13**, RAA_4), four or eight DSLs (**14**, DSL_4; **15**, DSL_8), four DSL-arginines (**16**, $RDSL_4$), and four or eight myristic acids (**17**, MA_4; **18**, MA_8, Figure 3, Schemes S1, S7, and S8). An overview of CPS with different transporters, CPS complexes with different substrates, and controls described in the following is provided in Figure 3. A comprehensive summary of all structures used can be found in Figure S39, Supporting Information.

Cytosolic Delivery of CPS Evidenced by HC-CAPA. CAPA has been introduced recently by the Kritzer group to

https://dx.doi.org/10.1021/jacs.9b13621
J. Am. Chem. Soc. 2020, 142, 4784−4792

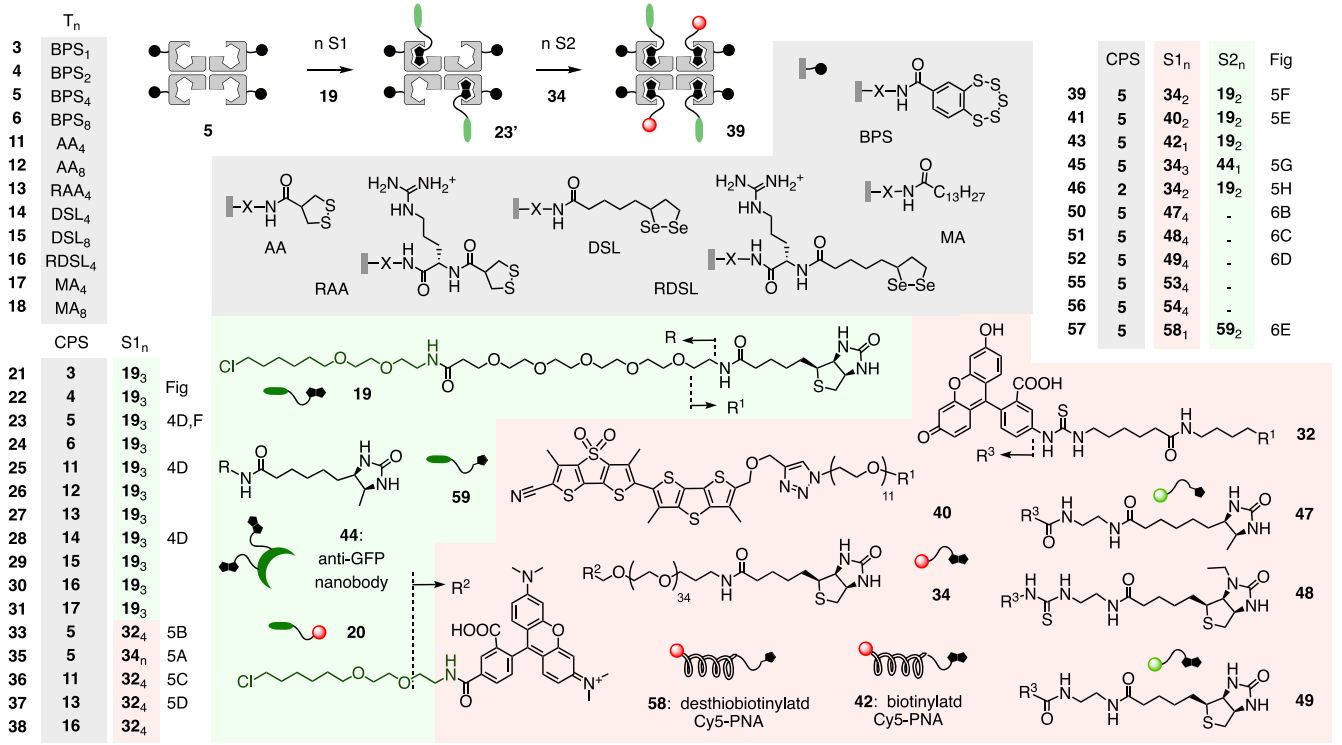

Figure 3. Structure of monomers, CPS with *n* transporters T, CPS complexes with *n* substrates S1 and S2, and controls made and used in this study with representative assembly of **39** and indication of pertinent figures (Fig) reporting on activity. *n* is the stoichiometry used for complex preparation (**35**: *n* = 2−4, see text); **47** and **49** are a mixture of *m*/*p*-carboxyfluorescein isomers.

quantify cytosolic delivery reliably based on function.[25] This is important because the commonly used fluorescence intensity-based assays are often significantly affected by the environment[2,11−15] and, in general, demonstrate neither cytosolic location nor intact functionality.[25,26] CAPA operates with HGM cells, e.g., HeLa cells that have a fusion protein of HaloTag and GFP (Figure 4F, green) expressed on the outer surface of mitochondria (Figure 4A).[25,30] Delivered chloroalkanes, such as **19**, react in cytosol with HaloTags (Figure 4B) and thus inhibit reaction with the subsequently added fluorescent chloroalkane **20** (Figure 4C and 4H vs 4I, red). Thus, the delivery of chloroalkanes can be quantified from the fluorescence intensity of **20** on mitochondria. To secure quantitative data of the highest possible quality, we adapted CAPA to an image-based assay using automated high-content fluorescence microscopy (referred to also as high-content screening (HCS) or high-content analysis (HCA)),[27] preserving the power of flow cytometry to record and analyze thousands of cells in a short period of time without losing the subcellular spatial resolution of fluorescence imaging. For HC-CAPA, the mitochondria with HaloTags were first segmented applying a *top-hat* transform to the unmodifiable fluorescence of the GFP (Figure 4F). Then this mask was used to collect the intensity of **20** only in the region of mitochondria, thus excluding any possible false positives from off-target signals (Figure 4G, Figures S2−S5).

The newly devised HC-CAPA was then used to assess cytosolic delivery of CPS-chloroalkane complexes **21**−**31**, prepared by mixing the corresponding CPS with biotinylated chloroalkane **19** (Figure 3, Scheme S9). The absence of unbound **19** was assured using a substoichiometric 3 equiv of ligand per CPS and by meticulous purification using centrifugal filters. Results from HC-CAPA were quantified as CP_{50}, which is the CPS concentration needed for 50% inhibition of HaloTagging by rhodamine **20**. The best CP_{50} = 2.1 ± 0.3 μM was found for BPS_4 **23**, with the onset of activity detectable already in the nanomolar range (Figures 4D (●), 4E, and 4I). This activity exceeded the CP_{50} = 3.1 ± 0.5 μM reported for chloroalkane-tagged Tat peptide, the original CPP from the HIV virus.[25] Although direct quantitative comparison of these two values has to be made with due caution considering the different methods used for data collection, it perfectly illustrates the high efficiency of cytosolic delivery with BPS_4 **23**. BPS together with a large 52 kDa protein outperforming this small undecapeptide in cytosolic delivery is particularly interesting considering that uptake efficiencies in general decrease rapidly with increasing substrate size.[5,8,9,11]

The presence of fewer and more transporters in BPS_1 **21**, BPS_2 **22**, and BPS_8 **24** reduced activity (Figure 4E). The second best COC was AA with CP_{50} = 8 ± 1 μM for AA_8 **26** and CP_{50} = 14.9 ± 0.5 μM for AA_4 **25**, followed by DSL_4 **28** with CP_{50} = 34 ± 6 μM (Figures 4D−I). The presence of more transporters in DSL_8 **29** rather deteriorated the poor performance of DSL under these conditions. Insertion of guanidinium cations between the protein and COCs in RAA_4 **27** and $RDSL_4$ **30** was also ineffective in improving the transport activity, thus excluding contributions from CPP-like mechanisms[7−11] (CP_{50} = 20 ± 1 μM for **27**, >35 μM for **30**). Decreasing activities from BPS_4 **23** to BPS_8 **24** but not from AA_4 **25** to AA_8 **26** suggested that the higher hydrophobicity of BPS starts to hinder thiol-mediated uptake in the presence of more than four transporters per streptavidin, possibly due to decreasing solubility in water, aggregation, and even precipitation (Figure 4E). The best activity found with an intermediate number of BPS, or "Goldilocks" behavior,[31] implied that the right balance between sufficient hydrophilicity

https://dx.doi.org/10.1021/jacs.9b13621
J. Am. Chem. Soc. 2020, 142, 4784−4792

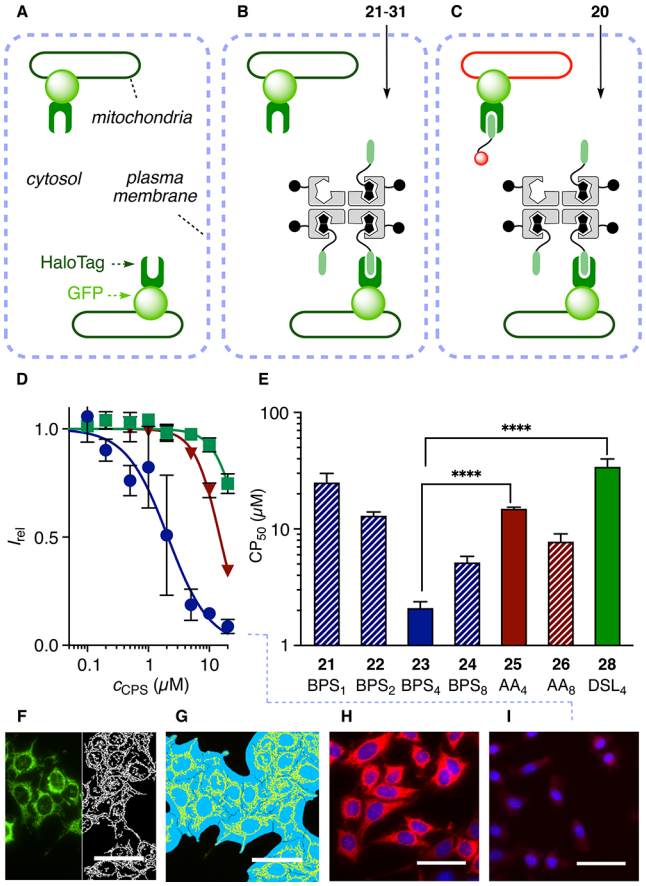

Figure 4. (A–C) Schematic representation of CAPA: (A) HGM cells were incubated with (B) **21**–**31** and then (C) **20**. (D) HC-CAPA dose–response curves for **23** (●), **25** (▼), and **28** (■). (E) CP_{50} values of **21**–**26** and **28**. Statistical significance (**** $p < 0.0001$) was estimated by the *t* test using GraphPad Prism. (F–I) Representative images for HC-CAPA: (F) *top-hat* transform (white) of the image generated from the emission of GFP (green); (G) cell body (light blue) and mitochondria (yellow) masks applied to selectively extract from the mitochondria the emission intensity in the rhodamine channel; (H) rhodamine channel (red) from labeling with **20** without incubation with transporters and (I) after incubation with 20 μM **23** (nuclei in blue; Hoechst 33342, poststaining, scale bars 50 μm).

and number of transporters is rather subtle. Goldilocks behavior further supported that simple passive diffusion does not account for the top activity of BPS_4 **23**. Corroborative experimental support for this important conclusion was secured with myristyl control MA_4 **31**, which is as hydrophobic as BPS but completely inactive (Figure S6, Table S3, and Scheme S9).

We previously reported the mechanistic insights in support of thiol-mediated uptake of BPS, including partial inhibition with Ellman's reagent which inactivates cell surface thiols, insensitivity toward endocytosis inhibitors (cytochalasin B, wortmannin, chlorpromazine, or methyl-β-cyclodextrin), the formation of complex adaptive networks of extreme sulfur species in the presence of thiols and disulfides (up to heptamers **1**, Figure 1D), and stability in PBS buffer for >2 weeks.[15] In the current context focusing on cell-penetrating streptavidin, which is a general and unrestricted availability of biotin–streptavidin biotechnology for cellular uptake independent of the transporter used, repetition of these mechanistic studies on BPS-mediated uptake was less relevant and off topic. Nevertheless, retention on and thiol-meditated release from thiol-affinity columns, arguably the most compelling test for thiol-mediated uptake,[14a,15] was confirmed for intact BPS_4 **23** (Figure S7). As previously noted with AA,[12] the presence of 10% serum in Leibovitz's media did not affect the activity much, resulting in a less than doubled CP_{50} of BPS_4 **23**.

Targetless Delivery of CPS into Various Cells. The delivery of four biotinylated fluoresceins **32**[14] in BPS_4 **33** into unmodified HeLa cells afforded confocal laser scanning microscopy (CLSM) images with diffusely emitting cells, including their nuclei (Figures 5B and S8).[15] Similar images

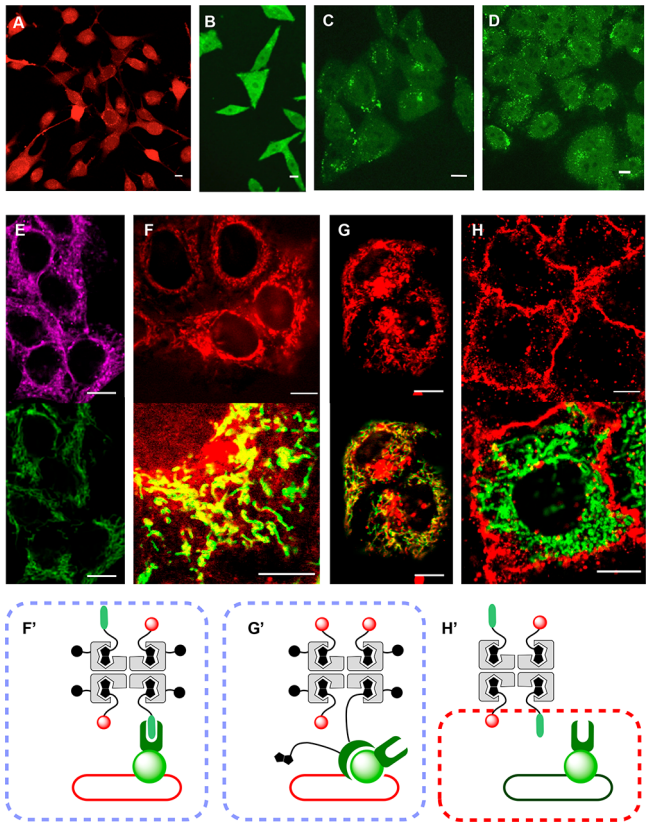

Figure 5. CLSM images of (A) C2C12 cells after incubation with fluorescently labeled BPS_4 **35** (n_{34} = 2, 10 μM, 2 h), of HeLa cells after incubation with (B) BPS_4 **33**, (C) AA_4 **36**, and (D) RAA_4 **37** (all 10 μM, 8 h), and of HGM cells after incubation with (E) BPS_4 **41** (emission top, **40**; bottom, GFP; 5 μM, 2 h), (F) **39** (top, **34**; bottom, **34** (red) + GFP (green), 5 μM, 2 h), (G) **45** (top, **34**; bottom, **34** (red) + GFP (green), 2.5 μM, 2 h), and (H) **46** (top, **40**; bottom, **40** (red) + GFP (green), 5 μM, 2 h) in Leibovitz's media; complex stoichiometry indicates the ratios of preparation. (F′–H′) Design of experiments F–H. Scale bars: 10 μm.

were obtained with biotinylated rhodamine **34**[2] in BPS_4 **35** inside C2C12, HeLa, MCF7, or MDCK cells (Figures 5A and S9; n_{34} = 2). Weaker fluorescence was observed in CLSM images of AA_4 **36** in HeLa cells (Figure 5C). The added cations in RAA_4 **37** and $RDSL_4$ **38** did not help to improve the activity significantly, confirming that CPP-like mechanisms[7−11] are negligible for COC-mediated uptake (Figures 5D and S8). Contrary to BPS_4 **33**, images of AA_4 **36** and RAA_4 **37** contain bright punctate patterns on a diffuse background, which usually indicate contributions from endolysosomes and perhaps also

https://dx.doi.org/10.1021/jacs.9b13621
J. Am. Chem. Soc. 2020, 142, 4784−4792

precipitating aggregates besides emission from the cytosol. With flow cytometry, such contributions from endosomal capture are recorded as false positives. The here introduced HC-CAPA is powerful because all eventual false positives[25,26] are eliminated without losses in fast acquisition of statistically relevant high-content data.

Targeted Delivery of Fluorophores, Nanobodies, and PNA. Using the best CPS, that is, BPS_4 **5**, we explored the simultaneous delivery of two functions, here a reporter and a targeting unit. BPS_4 **5** was loaded with biotinylated chloroalkane **19** and rhodamine **34** (Figures 3 and 5F′, Scheme S12). Incubation of HeLa cells expressing HaloTags on mitochondria with the resulting complex **39** afforded CLSM images with fluorescently labeled mitochondria (Figure 5F, top). The diffuse emission from cytosol and nuclei observed without targeting (Figures 5A and 5B) disappeared, thus confirming that delivery of complex **39** to the HaloTag on the surface of mitochondria is as specific as expected. A good colocalization with GFP emission demonstrated the targeted delivery of the complex to HaloTags (Figures 5F, bottom, S10A, and S10B). HaloTag targeting was substrate independent; the substitution of rhodamine **34** with flipper **40**[29] gave similar images for delivery of the respective complex **41** to HaloTags on mitochondria (Figures 3, 5E, and S11). This result was of interest for the fluorescence imaging of precisely localized membrane tension within living cells.[29] Targeted delivery of biotinylated and Cy5-labeled 18-mer PNA **42**[28] in complex **43** was also accomplished in HGM cells (vide infra, Figure S13).

Biotinylated anti-GFP nanobodies[8] **44** were probed as alternative targeting units in complex **45**, recognizing GFP instead of HaloTag of the fusion protein on mitochondria. The resulting images showed good colocalization with GFP together with less important endolysosomal capture and/or precipitates (red dots, Figures 5G and S12). These off-targeted, endolysosomal capture and/or precipitates probably originate from the larger oligomers of complex **45** cross-linked through the multivalent anti-GFP nanobodies[8] **44** with more than one biotin (Figures 3 and 5G′). Shifts in uptake mechanism from cytosolic delivery to endosomal capture have been observed frequently with increasing substrate size, although much more for CPPs[5] than for thiol-mediated uptake.[8,9,11] To minimize these side effects, complex **45** was prepared by incubation of BPS_4 **5** with 3 equiv of fluorophores **34** before incubation with the multivalent nanobodies **44**, a procedure that should in turn increase formation of the targetless CPS side product **35** loaded with four fluorophores **34** only (Figure 3, n_{34} = 4). However, eventual contributions from off-targeted delivery with CPS **35** were very minor (diffuse red as in Figures 5A, 5G, and S12). Considering this situation, the targeted delivery mediated by anti-GFP nanobodies[8] **44** to GFP expressed on the surface of mitochondria was remarkably efficient and supported, with red fluorescence originating from ligand **34**, that the majority of complex **45** reaches the cytosol in intact functional form (yellow, Figures 5G, 5G′, and S12). The control complex **46** without COCs was unable to penetrate cells and showed no colocalization with GFP (Figures 5H, S10C, and S10D).

Controlled Intracellular Release of Substrates from CPS. Once delivered in the cells, the substrate would ideally be detached from transporter and target at a well-defined time[16] to ensure and follow its proper function on demand (Figure 1D). To elaborate on the timed release of substrates from CPS, fluorescein as a responsive model substrate was equipped with desthiobiotin **47**, *N*-ethylbiotin **48**, and biotin **49** (Figures 3 and 6, Schemes S4 and S13). Desthiobiotin (K_d = 10^{-11} M)[3]

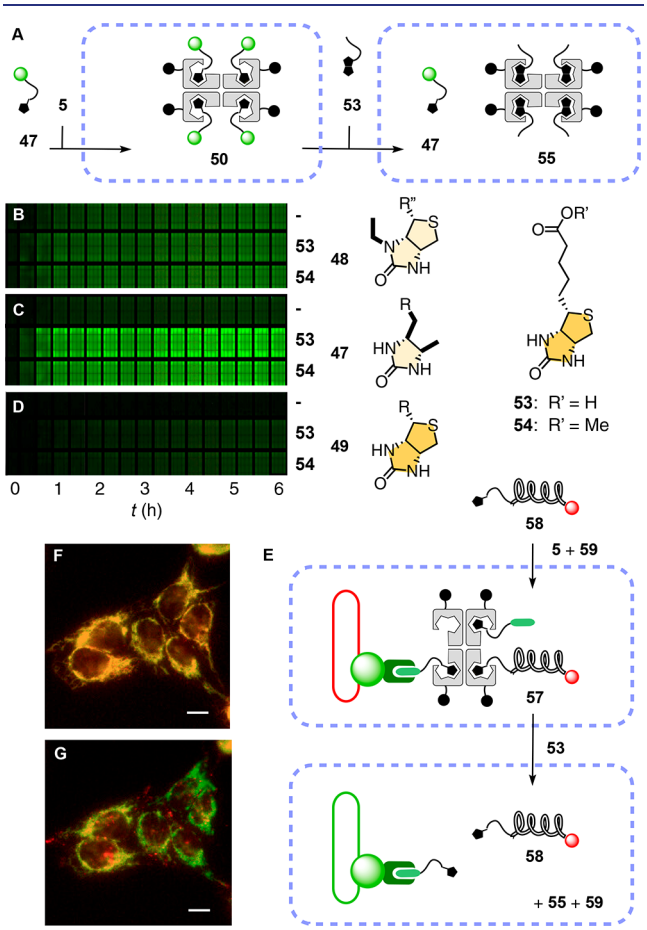

Figure 6. (A) Delivery of **47** with BPS_4 **5** followed by addition of biotin **53** to release **47** from complex **50** in the cytosol. (B–D) Original image of the multiwell plate to monitor the time course of substrate release in HeLa cells by automated high-content fluorescence microscopy. Thousands of cells preincubated with (B) **51**, (C) **50**, or (D) **52** (10 μM, 6 h in Leibovitz's medium) were treated with **53** (middle), **54** (bottom; 40 μM each), or none (top) and imaged every 12 min (left to right; shown are every other images). (E–G) Spatiotemporal control of (F) the delivery of **58** with **5** and **59** to the mitochondria of HGM cells (5 μM, 2 h incubation in Leibovitz's medium) and (G) the release of **58** after addition of **53** (**58** (red) + GFP (green), 40 μM). Scale bars: 10 μm.

and *N*-ethylbiotin (K_d = 10^{-9} M)[4] bind to streptavidin but with reduced affinity compared to biotin (K_d = 10^{-15} M).[3,4] The corresponding complexes **50**–**52** were readily accessible by incubation with BPS_4 **5** (Figures 3 and 6).

Desthiobiotin **47** was first delivered in complex **50**; then biotin **53**, a nontoxic vitamin, or its methyl ester **54** was added at a 40 μM concentration as recommended by the RUSH technology[16] to diffuse into the cell, exchange, and release substrate **47** in the cytosol (Figure 6A). As streptavidin strongly quenches the fluorescence of bound carboxyfluorescein,[2] intracellular desthiobiotin–biotin exchange was detectable by fluorescence recovery of the released substrate **47**, whereas the biotin–streptavidin side product **55** or **56** passes undetected.

https://dx.doi.org/10.1021/jacs.9b13621
J. Am. Chem. Soc. 2020, 142, 4784–4792

Quantitative release kinetics were obtained by automated high-content fluorescence microscopy of wells containing thousands of cells with an increasing incubation time with biotin **53** and its methyl ester **54** (Figures 6B–D and S14). Identical t_{50} = 17 min obtained for controlled release of desthiobiotin **47** from CPS **50** with **53** and **54** demonstrated that passive diffusion of the protonatable carboxylate **53** into the cell is not rate limiting (Figures 6C and S14). In clear contrast, the release of *N*-ethylbiotin **48** from complex **51** was spontaneous and not affected by the presence of either **53** or **54** (Figure 6B). The lower fluorescence intensity observed with **48** (Figure 6B) compared with **47** (Figure 6C) suggested that **48** dissociated from CPS already during incubation time, diffused out of cells, and was washed away before the start of the acquisition (Figure S14C). Similar spontaneous release of desthiobiotin **47** was slow on the time scale of biotin-controlled release (Figures 6C and S14B). This difference in spontaneous release was in agreement with the poorer binding affinity of *N*-ethylbiotin **48** (K_d = 10^{-9} M)[4] compared to desthiobiotin **47** (K_d = 10^{-11} M).[3] On the other hand, the controlled release of **49** from **52** by biotin–biotin exchange was negligible even after an extended incubation period (Figure 6D), consistent with much stronger binding of biotin **49** compared to desthiobiotin **47**. Insufficient release of biotin **49** and excessive release of *N*-ethylbiotin **48** added up again in Goldilocks behavior,[31] identifying desthiobiotin **47** with neither too strong nor too weak binding as the ligand of choice for controlled release within cells.

To finally combine targeted delivery and controlled release, PNA was selected as a prototypical example of a useful reagent that has been limited in scope by its cellular permeability.[28] In complex **57**, CPS **5** was loaded with desthiobiotinylated 18-mer PNA **58** and chloroalkane **59** (Figures 3 and 6E, Schemes S5, S6, and S13). The good colocalization (yellow) of Cy5 attached to PNA **58** (red) and GFP (green) demonstrated targeted delivery of complex **57** to HaloTags on the mitochondria of HGM cells in intact form and with excellent selectivity (Figures 6F and S15). Subsequent addition of biotin **53** induced PNA release, detectable as weakened emission of Cy5 on the mitochondria due to dilution of the liberated PNA **58** into the cytosol (Figures 6G, 6E, and S15). These results thus supported the compatibility of CPS delivery with spatiotemporal control using biotin analogs.[16]

CONCLUSION

This study introduces CPS as a privileged scaffold for cellular uptake, simple and robust, with biotin–streptavidin technology made fully available for general bifunctional delivery with spatiotemporal control. HC-CAPA, the recent CAPA[25] combined with automated high-content fluorescence microscopy[27] is devised as the method of choice to quantify cytosolic delivery; the currently emerging benzopolysulfanes[15] are validated as COCs of choice for cytosolic delivery. Their performance supports the integration of increasingly unorthodox[32] oligochalcogenide exchange chemistry to find new ways to enter into cells and encourages studies on mechanistic hypotheses, i.e., molecular walkers and dynamic-covalent adaptive networks.[14,15,19–22]

ASSOCIATED CONTENT

Supporting Information

The Supporting Information is available free of charge at https://pubs.acs.org/doi/10.1021/jacs.9b13621.

Materials and methods; small-molecule synthesis; cell lines and plasmids; CPS synthesis; combining CAPA with automated HC microscopy; cellular uptake of CPS; targeted delivery; supporting references; NMR spectra; characterization of PNA derivatives; summary of structures (PDF)

AUTHOR INFORMATION

Corresponding Authors

Javier López-Andarias − *School of Chemistry and Biochemistry and National Centre of Competence in Research (NCCR) Chemical Biology, University of Geneva, Geneva 1211, Switzerland*; Email: javier.lopez@unige.ch

Stefan Matile − *School of Chemistry and Biochemistry and National Centre of Competence in Research (NCCR) Chemical Biology, University of Geneva, Geneva 1211, Switzerland*; orcid.org/0000-0002-8537-8349; Email: stefan.matile@unige.ch

Authors

Jacques Saarbach − *School of Chemistry and Biochemistry and National Centre of Competence in Research (NCCR) Chemical Biology, University of Geneva, Geneva 1211, Switzerland*

Dimitri Moreau − *School of Chemistry and Biochemistry and National Centre of Competence in Research (NCCR) Chemical Biology, University of Geneva, Geneva 1211, Switzerland*

Yangyang Cheng − *School of Chemistry and Biochemistry and National Centre of Competence in Research (NCCR) Chemical Biology, University of Geneva, Geneva 1211, Switzerland*

Emmanuel Derivery − *MRC Laboratory of Molecular Biology, Cambridge CB2 0QH, United Kingdom*; orcid.org/0000-0003-3927-5944

Quentin Laurent − *School of Chemistry and Biochemistry and National Centre of Competence in Research (NCCR) Chemical Biology, University of Geneva, Geneva 1211, Switzerland*

Marcos González-Gaitán − *School of Chemistry and Biochemistry and National Centre of Competence in Research (NCCR) Chemical Biology, University of Geneva, Geneva 1211, Switzerland*

Nicolas Winssinger − *School of Chemistry and Biochemistry and National Centre of Competence in Research (NCCR) Chemical Biology, University of Geneva, Geneva 1211, Switzerland*; orcid.org/0000-0003-1636-7766

Naomi Sakai − *School of Chemistry and Biochemistry and National Centre of Competence in Research (NCCR) Chemical Biology, University of Geneva, Geneva 1211, Switzerland*

Complete contact information is available at: https://pubs.acs.org/10.1021/jacs.9b13621

Notes

The authors declare no competing financial interest.

ACKNOWLEDGMENTS

This paper is dedicated to George Whitesides on the occasion of his 80th birthday. We thank E. Bartolami, A. Goujon, R. Martinent, and K. Strakova for contributions to CPS synthesis, H. Riezman, N. Jiménez-Rojo, and S. Vossio for help with plasmid amplification, J. A. Kritzer (Tufts) for providing materials, the NMR, the MS, and the Bioimaging platforms for services, and the University of Geneva, the NCCR Chemical Biology, the NCCR Molecular Systems Engineering, and the

Swiss NSF for financial support. J.L.A. acknowledges a Curie fellowship (740288).

REFERENCES

(1) (a) Wilson, M. E.; Whitesides, G. M. Conversion of a Protein to a Homogeneous Asymmetric Hydrogenation Catalyst by Site-Specific Modification with a Diphosphinerhodium(I) Moiety. *J. Am. Chem. Soc.* **1978**, *100*, 306−307. (b) Schreiber, C. L.; Smith, B. D. Molecular Conjugation Using Non-Covalent Click Chemistry. *Nat. Rev. Chem.* **2019**, *3*, 393−400. (c) Dundas, C. M.; Demonte, D.; Park, S. Streptavidin−Biotin Technology: Improvements and Innovations in Chemical and Biological Applications. *Appl. Microbiol. Biotechnol.* **2013**, *97*, 9343−9353. (d) Sun, X.; Montiel, D.; Li, H.; Yang, H. Plug-and-Go" Strategy to Manipulate Streptavidin Valencies. *Bioconjugate Chem.* **2014**, *25*, 1375−1380. (e) Heinisch, T.; Ward, T. R. Artificial Metalloenzymes Based on the Biotin−Streptavidin Technology: Challenges and Opportunities. *Acc. Chem. Res.* **2016**, *49*, 1711−1721. (f) Dubacheva, G. V.; Araya-Callis, C.; Geert Volbeda, A.; Fairhead, M.; Codee, J.; Howarth, M.; Richter, R. P. Controlling Multivalent Binding through Surface Chemistry: Model Study on Streptavidin. *J. Am. Chem. Soc.* **2017**, *139*, 4157−4167.

(2) Gruber, H. J.; Marek, M.; Schindler, H.; Kaiser, K. Biotin−Fluorophore Conjugates with Poly(Ethylene Glycol) Spacers Retain Intense Fluorescence after Binding to Avidin and Streptavidin. *Bioconjugate Chem.* **1997**, *8*, 552−559.

(3) (a) Ding, Y.; Williams, N. H.; Hunter, C. A. A Synthetic Vesicle-to-Vesicle Communication System. *J. Am. Chem. Soc.* **2019**, *141*, 17847−17853. (b) Sadhu, K. K.; Eierhoff, T.; Römer, W.; Winssinger, N. Photoreductive Uncaging of Fluorophore in Response to Protein Oligomers by Templated Reaction in Vitro and in Cellulo. *J. Am. Chem. Soc.* **2012**, *134*, 20013−20016. (c) Osuna Gálvez, A.; Bode, J. W. Traceless Templated Amide-Forming Ligations. *J. Am. Chem. Soc.* **2019**, *141*, 8721−8726.

(4) Ying, L.-Q.; Branchaud, B. P. Design of a Reversible Biotin Analog and Applications in Protein Labeling, Detection, and Isolation. *Chem. Commun.* **2011**, *47*, 8593−8595.

(5) (a) Juanes, M.; Lostalé-Seijo, I.; Granja, J. R.; Montenegro, J. Supramolecular Recognition and Selective Protein Uptake by Peptide Hybrids. *Chem. - Eur. J.* **2018**, *24*, 10689−10698. (b) Kuan, S. L.; Ng, D. Y. W.; Wu, Y.; Förtsch, C.; Barth, H.; Doroshenko, M.; Koynov, K.; Meier, C.; Weil, T. pH Responsive Janus-like Supramolecular Fusion Proteins for Functional Protein Delivery. *J. Am. Chem. Soc.* **2013**, *135*, 17254−17257. (c) Li, S.-D.; Huang, L. Targeted Delivery of Antisense Oligodeoxynucleotide and Small Interference RNA into Lung Cancer Cells. *Mol. Pharmaceutics* **2006**, *3*, 579−588. (d) Lee, H.; Kim, T. H.; Park, T. G. A Receptor-Mediated Gene Delivery System Using Streptavidin and Biotin-Derivatized, Pegylated Epidermal Growth Factor. *J. Controlled Release* **2002**, *83*, 109−119.

(6) Ulrich, S. Growing Prospects of Dynamic Covalent Chemistry in Delivery Applications. *Acc. Chem. Res.* **2019**, *52*, 510−519.

(7) (a) Bang, E.-K.; Gasparini, G.; Molinard, G.; Roux, A.; Sakai, N.; Matile, S. Substrate-Initiated Synthesis of Cell-Penetrating Poly(disulfide)s. *J. Am. Chem. Soc.* **2013**, *135*, 2088−2091. (b) Qian, L.; Fu, J.; Yuan, P.; Du, S.; Huang, W.; Li, L.; Yao, S. Q. Intracellular Delivery of Native Proteins Facilitated by Cell-Penetrating Poly(disulfide)s. *Angew. Chem., Int. Ed.* **2018**, *57*, 1532−1536. (c) Yuan, P.; Mao, X.; Wu, X.; Liew, S. S.; Li, L.; Yao, S. Q. Mitochondria-Targeting, Intracellular Delivery of Native Proteins Using Biodegradable Silica Nanoparticles. *Angew. Chem., Int. Ed.* **2019**, *58*, 7657−7661. (d) Liu, Y.; Jia, Y.; Wu, Q.; Moore, J. S. Architecture-Controlled Ring-Opening Polymerization for Dynamic Covalent Poly(Disulfide)s. *J. Am. Chem. Soc.* **2019**, *141*, 17075−17080. (e) Zhang, X.; Waymouth, R. M. 1,2-Dithiolane-Derived Dynamic, Covalent Materials: Cooperative Self-Assembly and Reversible Cross-Linking. *J. Am. Chem. Soc.* **2017**, *139*, 3822−3833. (f) Zhang, Q.; Deng, Y. X.; Luo, H. X.; Shi, C. Y.; Geise, G. M.; Feringa, B. L.; Tian, H.; Qu, D. H. Assembling a Natural Small Molecule into a Supramolecular Network with High Structural Order and Dynamic Functions. *J. Am. Chem. Soc.* **2019**, *141*, 12804−12814. (g) Okamoto, Y.; Kojima, R.; Schwizer, F.; Bartolami, E.; Heinisch, T.; Matile, S.; Fussenegger, M.; Ward, T. R. A Cell-Penetrating Artificial Metalloenzyme Regulates a Gene Switch in a Designer Mammalian Cell. *Nat. Commun.* **2018**, *9*, 1943.

(8) Derivery, E.; Bartolami, E.; Matile, S.; Gonzalez-Gaitan, M. Efficient Delivery of Quantum Dots into the Cytosol of Cells Using Cell-Penetrating Poly(disulfide)s. *J. Am. Chem. Soc.* **2017**, *139*, 10172−10175.

(9) (a) Meng, X.; Li, T.; Zhao, Y.; Wu, C. CXC-Mediated Cellular Uptake of Miniproteins: Forsaking "Arginine Magic. *ACS Chem. Biol.* **2018**, *13*, 3078−3086. (b) Shu, Z.; Tanaka, I.; Ota, A.; Fushihara, D.; Abe, N.; Kawaguchi, S.; Nakamoto, K.; Tomoike, F.; Tada, S.; Ito, Y.; Kimura, Y.; Abe, H. Disulfide-Unit Conjugation Enables Ultrafast Cytosolic Internalization of Antisense DNA and SiRNA. *Angew. Chem., Int. Ed.* **2019**, *58*, 6611−6615. (c) Zhou, J.; Sun, L.; Wang, L.; Liu, Y.; Li, J.; Li, J.; Li, J.; Yang, H. Self-Assembled and Size-Controllable Oligonucleotide Nanospheres for Effective Antisense Gene Delivery through an Endocytosis-Independent Pathway. *Angew. Chem., Int. Ed.* **2019**, *58*, 5236−5240.

(10) (a) Torres, A. G.; Gait, M. J. Exploiting Cell Surface Thiols to Enhance Cellular Uptake. *Trends Biotechnol.* **2012**, *30*, 185−190. (b) Oupický, D.; Li, J. Bioreducible Polycations in Nucleic Acid Delivery: Past, Present, and Future Trends. *Macromol. Biosci.* **2014**, *14*, 908−922. (c) Du, S.; Liew, S. S.; Li, L.; Yao, S. Q. Bypassing Endocytosis: Direct Cytosolic Delivery of Proteins. *J. Am. Chem. Soc.* **2018**, *140*, 15986−15996. (d) Aubry, S.; Burlina, F.; Dupont, E.; Delaroche, D.; Joliot, A.; Lavielle, S.; Chassaing, G.; Sagan, S. Cell-Surface Thiols Affect Cell Entry of Disulfide-Conjugated Peptides. *FASEB J.* **2009**, *23*, 2956−2967. (e) Hashim, P. K.; Okuro, K.; Sasaki, S.; Hoashi, Y.; Aida, T. Reductively Cleavable Nanocaplets for siRNA Delivery by Template-Assisted Oxidative Polymerization. *J. Am. Chem. Soc.* **2015**, *137*, 15608−15611. (f) Balakirev, M.; Schoehn, G.; Chroboczek, J. Lipoic Acid-Derived Amphiphiles for Redox-Controlled DNA Delivery. *Chem. Biol.* **2000**, *7*, 813−819. (g) Brülisauer, L.; Kathriner, N.; Prenrecaj, M.; Gauthier, M. A.; Leroux, J.-C. Tracking the Bioreduction of Disulfide-Containing Cationic Dendrimers. *Angew. Chem., Int. Ed.* **2012**, *51*, 12454−12458. (h) Drake, C. R.; Aissaoui, A.; Argyros, O.; Thanou, M.; Steinke, J. H. G.; Miller, A. D. Examination of The Effect of Increasing the Number of Intra-Disulfide Amino Functional Groups on the Performance of Small Molecule Cyclic Polyamine Disulfide Vectors. *J. Controlled Release* **2013**, *171*, 81−90. (i) Schneider, A. F. L.; Wallabregue, A. L. D.; Franz, L.; Hackenberger, C. P. R. Targeted Subcellular Protein Delivery Using Cleavable Cyclic Cell-Penetrating Peptides. *Bioconjugate Chem.* **2019**, *30*, 400−404. (j) Bode, S. A.; Wallbrecher, R.; Brock, R.; van Hest, J. C. M.; Löwik, D. W. P. M. Activation of Cell-Penetrating Peptides by Disulfide Bridge Formation of Truncated Precursors. *Chem. Commun.* **2014**, *50*, 415−417.

(11) (a) Gasparini, G.; Sargsyan, G.; Bang, E.-K.; Sakai, N.; Matile, S. Ring Tension Applied to Thiol-Mediated Cellular Uptake. *Angew. Chem., Int. Ed.* **2015**, *54*, 7328−7331. (b) Tirla, A.; Rivera-Fuentes, P. Peptide Targeting of an Intracellular Receptor of the Secretory Pathway. *Biochemistry* **2019**, *58*, 1184−1187. (c) Li, X.; Hou, Y.; Meng, X.; Ge, C.; Ma, H.; Li, J.; Fang, J. Selective Activation of a Prodrug by Thioredoxin Reductase Providing a Strategy to Target Cancer Cells. *Angew. Chem., Int. Ed.* **2018**, *57*, 6141−6145. (d) Chuard, N.; Gasparini, G.; Moreau, D.; Lörcher, S.; Palivan, C.; Meier, W.; Sakai, N.; Matile, S. Strain-Promoted Thiol-Mediated Cellular Uptake of Giant Substrates: Liposomes and Polymersomes. *Angew. Chem., Int. Ed.* **2017**, *56*, 2947−2950. (e) Singh, R.; Whitesides, G. M. Degenerate Intermolecular Thiolate-Disulfide Interchange Involving Cyclic Five-Membered Disulfides Is Faster by $\sim 10^3$ Than That Involving Six- or Seven-Membered Disulfides. *J. Am. Chem. Soc.* **1990**, *112*, 6304−6309.

(12) Abegg, D.; Gasparini, G.; Hoch, D. G.; Shuster, A.; Bartolami, E.; Matile, S.; Adibekian, A. Strained Cyclic Disulfides Enable Cellular Uptake by Reacting with the Transferrin Receptor. *J. Am. Chem. Soc.* **2017**, *139*, 231−238.

https://dx.doi.org/10.1021/jacs.9b13621
J. Am. Chem. Soc. 2020, 142, 4784−4792

(13) Zong, L.; Bartolami, E.; Abegg, D.; Adibekian, A.; Sakai, N.; Matile, S. Epidithiodiketopiperazines: Strain-Promoted Thiol-Mediated Cellular Uptake at the Highest Tension. *ACS Cent. Sci.* **2017**, *3*, 449−453.
(14) (a) Chuard, N.; Poblador-Bahamonde, A. I.; Zong, L.; Bartolami, E.; Hildebrandt, J.; Weigand, W.; Sakai, N.; Matile, S. Diselenolane-Mediated Cellular Uptake. *Chem. Sci.* **2018**, *9*, 1860−1866. (b) Bartolami, E.; Basagiannis, D.; Zong, L.; Martinent, R.; Okamoto, Y.; Laurent, Q.; Ward, T. R.; Gonzalez-Gaitan, M.; Sakai, N.; Matile, S. Diselenolane-Mediated Cellular Uptake: Efficient Cytosolic Delivery of Probes, Peptides, Proteins, Artificial Metalloenzymes and Protein-Coated Quantum Dots. *Chem. - Eur. J.* **2019**, *25*, 4047−4051. (c) Laurent, Q.; Sakai, N.; Matile, S. The Opening of 1,2-Dithiolanes and 1,2-Diselenolanes: Regioselectivity, Rearrangements, and Consequences for Poly(disulfide)s, Cellular Uptake and the Pyruvate Dehydrogenase Complex. *Helv. Chim. Acta* **2019**, *102*, e1800209.
(15) Cheng, Y.; Zong, L.; López-Andarias, J.; Bartolami, E.; Okamoto, Y.; Ward, T. R.; Sakai, N.; Matile, S. Cell-Penetrating Dynamic-Covalent Benzopolysulfane Networks. *Angew. Chem., Int. Ed.* **2019**, *58*, 9522−9526.
(16) (a) Boncompain, G.; Divoux, S.; Gareil, N.; de Forges, H.; Lescure, A.; Latreche, L.; Mercanti, V.; Jollivet, F.; Raposo, G.; Perez, F. Synchronization of Secretory Protein Traffic in Populations of Cells. *Nat. Methods* **2012**, *9*, 493−498. (b) Terai, T.; Kohno, M.; Boncompain, G.; Sugiyama, S.; Saito, N.; Fujikake, R.; Ueno, T.; Komatsu, T.; Hanaoka, K.; Okabe, T.; Urano, Y.; Perez, F.; Nagano, T. Artificial Ligands of Streptavidin (ALiS): Discovery, Characterization, and Application for Reversible Control of Intracellular Protein Transport. *J. Am. Chem. Soc.* **2015**, *137*, 10464−10467.
(17) (a) Kuan, S. L.; Stöckle, B.; Reichenwallner, J.; Ng, D. Y. W.; Wu, Y.; Doroshenko, M.; Koynov, K.; Hinderberger, D.; Müllen, K.; Weil, T. Dendronized Albumin Core−Shell Transporters with High Drug Loading Capacity. *Biomacromolecules* **2013**, *14*, 367−376. (b) McNaughton, B. R.; Cronican, J. J.; Thompson, D. B.; Liu, D. R. Mammalian Cell Penetration, SiRNA Transfection, and DNA Transfection by Supercharged Proteins. *Proc. Natl. Acad. Sci. U. S. A.* **2009**, *106*, 6111−6116. (c) Mix, K. A.; Lomax, J. E.; Raines, R. T. Cytosolic Delivery of Proteins by Bioreversible Esterification. *J. Am. Chem. Soc.* **2017**, *139*, 14396−14398.
(18) (a) Andersen, K. A.; Smith, T. P.; Lomax, J. E.; Raines, R. T. Boronic Acid for the Traceless Delivery of Proteins into Cells. *ACS Chem. Biol.* **2016**, *11*, 319−323. (b) Jakka, S. R.; Govindaraj, V.; Mugesh, G. A Single Atom Change Facilitates the Membrane Transport of Green Fluorescent Proteins in Mammalian Cells. *Angew. Chem., Int. Ed.* **2019**, *58*, 7713−7717. (c) Pelegri-O'Day, E. M.; Maynard, H. D. Controlled Radical Polymerization as an Enabling Approach for the Next Generation of Protein-Polymer Conjugates. *Acc. Chem. Res.* **2016**, *49*, 1777−1785. (d) Hou, Y.; Zhou, Y.; Wang, H.; Sun, J.; Wang, R.; Sheng, K.; Yuan, J.; Hu, Y.; Chao, Y.; Liu, Z.; Lu, H. Therapeutic Protein PEPylation: The Helix of Nonfouling Synthetic Polypeptides Minimizes Antidrug Antibody Generation. *ACS Cent. Sci.* **2019**, *5*, 229−236. (e) Velonia, K. Protein - Polymer Amphiphilic Chimeras: Recent Advances and Future Challenges. *Polym. Chem.* **2010**, *1*, 944−952.
(19) Beld, J.; Woycechowsky, K.; Hilvert, D. Small-Molecule Diselenides Catalyze Oxidative Protein Folding *in Vivo*. *ACS Chem. Biol.* **2010**, *5*, 177−182.
(20) (a) Alvadia, C.; Lim, N. K.; Clerico Mosina, V.; Oostergetel, G. T.; Dutzler, R.; Paulino, C. Cryo-EM Structures and Functional Characterization of the Murine Lipid Scramblase TMEM16F. *eLife* **2019**, *8*, e44365. (b) Wu, J.; Yan, Z.; Li, Z.; Qian, X.; Lu, S.; Dong, M.; Zhou, Q.; Yan, N. Structure of the Voltage-Gated Calcium Channel Cav1.1 at 3.6 Å Resolution. *Nature* **2016**, *537*, 191−196. (c) Jing, S.; Trowbridge, I. S. Identification of the Intermolecular Disulfide Bonds of the Human Transferrin Receptor and its Lipid-Attachment Site. *EMBO J.* **1987**, *6*, 327−331. (d) Ali Khan, H.; Mutus, B. Protein Disulfide Isomerase: A Multifunctional Protein with Multiple Physiological Roles. *Front. Chem.* **2014**, *2*, 70.
(21) (a) Schmidt, D.; Jiang, Q. X.; MacKinnon, R. Lipid-Dependent Gating of a Voltage-Gated Potassium Channel. *Nature* **2006**, *444*, 775−779. (b) Sakai, N.; Matile, S. Anion-Mediated Transfer of Polyarginine Across Liquid and Bilayer Membranes. *J. Am. Chem. Soc.* **2003**, *125*, 14348−14356.
(22) Jiang, C.-S.; Müller, W. E. G.; Schröder, H. C.; Guo, Y.-W. Disulfide- and Multisulfide-Containing Metabolites from Marine Organisms. *Chem. Rev.* **2012**, *112*, 2179−2207.
(23) Behar, V.; Danishefsky, S. J. Total Synthesis of the Novel Benzopentathiepin Varacinium Trifluoroacetate: The Viability of "Varacin-Free Base". *J. Am. Chem. Soc.* **1993**, *115*, 7017−7018.
(24) Xu, J.; Chatterjee, M.; Baguley, T. D.; Brouillette, J.; Kurup, P.; Ghosh, D.; Kanyo, J.; Zhang, Y.; Seyb, K.; Ononenyi, C.; Foscue, E.; Anderson, G. M.; Gresack, J.; Cuny, G. D.; Glicksman, M. A.; Greengard, P.; Lam, T. L.; Tautz, L.; Nairn, A. C.; Ellman, J. A.; Lombroso, P. J. Inhibitor of the Tyrosine Phosphatase STEP Reverses Cognitive Deficits in a Mouse Model of Alzheimer's Disease. *PLoS Biol.* **2014**, *12*, e1001923.
(25) Peraro, L.; Deprey, K. L.; Moser, M. K.; Zou, Z.; Ball, H. L.; Levine, B.; Kritzer, J. A. Cell Penetration Profiling Using the Chloroalkane Penetration Assay. *J. Am. Chem. Soc.* **2018**, *140*, 11360−11369.
(26) (a) Deprey, K.; Becker, L.; Kritzer, J.; Plückthun, A. Trapped! A Critical Evaluation of Methods for Measuring Total Cellular Uptake versus Cytosolic Localization. *Bioconjugate Chem.* **2019**, *30*, 1006−1027. (b) Méndez-Ardoy, A.; Lostalé-Seijo, I.; Montenegro, J. Where in the Cell Is Our Cargo? Methods Currently Used to Study Intracellular Cytosolic Localisation. *ChemBioChem* **2019**, *20*, 488−498. (c) Lacroix, A.; Vengut-Climent, E.; de Rochambeau, D.; Sleiman, H. F. Uptake and Fate of Fluorescently Labeled DNA Nanostructures in Cellular Environments: A Cautionary Tale. *ACS Cent. Sci.* **2019**, *5*, 882−891.
(27) (a) Abraham, V. C.; Taylor, D. L.; Haskins, J. R. High Content Screening Applied to Large-Scale Cell Biology. *Trends Biotechnol.* **2004**, *22*, 15−22. (b) Eggert, U. S.; Mitchison, T. J. Small Molecule Screening by Imaging. *Curr. Opin. Chem. Biol.* **2006**, *10*, 232−237. (c) Moreau, D.; Gruenberg, J. Automated Microscopy and High Content Screens (Phenotypic Screens) in Academia Labs. *Chimia* **2016**, *70*, 878−882.
(28) (a) Saarbach, J.; Sabale, P. M.; Winssinger, N. Peptide Nucleic Acid (PNA) and Its Applications in Chemical Biology, Diagnostics, and Therapeutics. *Curr. Opin. Chem. Biol.* **2019**, *52*, 112−124. (b) Zhao, X.-L.; Chen, B.-C.; Han, J.-C.; Wei, L.; Pan, X.-B. Delivery of Cell-Penetrating Peptide-Peptide Nucleic Acid Conjugates by Assembly on an Oligonucleotide Scaffold. *Sci. Rep.* **2015**, *5*, 17640. (c) Wolfe, J. M.; Fadzen, C. M.; Choo, Z.-N.; Holden, R. L.; Yao, M.; Hanson, G. J.; Pentelute, B. L. Machine Learning to Predict Cell-Penetrating Peptides for Antisense Delivery. *ACS Cent. Sci.* **2018**, *4*, 512−520. (d) Dragulescu-Andrasi, A.; Rapireddy, S.; He, G.; Bhattacharya, B.; Hyldig-Nielsen, J. J.; Zon, G.; Ly, D. H. Cell-Permeable Peptide Nucleic Acid Designed to Bind to the 5′-Untranslated Region of E-Cadherin Transcript Induces Potent and Sequence-Specific Antisense Effects. *J. Am. Chem. Soc.* **2006**, *128*, 16104−16112. (e) Turner, J. J.; Ivanova, G. D.; Verbeure, B.; Williams, D.; Arzumanov, A. A.; Abes, S.; Lebleu, B.; Gait, M. J. Cell-Penetrating Peptide Conjugates of Peptide Nucleic Acids (PNA) as Inhibitors of HIV-1 Tat-Dependent Trans-Activation in Cells. *Nucleic Acids Res.* **2005**, *33*, 6837−6849.
(29) (a) Goujon, A.; Straková, K.; Sakai, N.; Matile, S. Streptavidin Interfacing as a General Strategy to Localize Fluorescent Membrane Tension Probes in Cells. *Chem. Sci.* **2019**, *10*, 310−319. (b) Goujon, A.; Colom, A.; Straková, K.; Mercier, V.; Mahecic, D.; Manley, S.; Sakai, N.; Roux, A.; Matile, S. Mechanosensitive Fluorescent Probes to Image Membrane Tension in Mitochondria, Endoplasmic Reticulum and Lysosomes. *J. Am. Chem. Soc.* **2019**, *141*, 3380−3384.
(30) (a) Los, G. V.; Encell, L. P.; McDougall, M. G.; Hartzell, D. D.; Karassina, N.; Zimprich, C.; Wood, M. G.; Learish, R.; Ohana, R. F.; Urh, M.; Simpson, D.; Mendez, J.; Zimmerman, K.; Otto, P.; Vidugiris, G.; Zhu, J.; Darzins, A.; Klaubert, D. H.; Bulleit, R. F.;

https://dx.doi.org/10.1021/jacs.9b13621
J. Am. Chem. Soc. 2020, 142, 4784−4792

Wood, K. V. HaloTag: A Novel Protein Labeling Technology for Cell Imaging and Protein Analysis. *ACS Chem. Biol.* **2008**, *3*, 373−382. (b) Long, M. J. C.; Poganik, J. R.; Aye, Y. On-Demand Targeting: Investigating Biology with Proximity-Directed Chemistry. *J. Am. Chem. Soc.* **2016**, *138*, 3610−3622. (c) Chambers, J. E.; Kubánková, M.; Huber, R. G.; López-Duarte, I.; Avezov, E.; Bond, P. J.; Marciniak, S. J.; Kuimova, M. K. An Optical Technique for Mapping Microviscosity Dynamics in Cellular Organelles. *ACS Nano* **2018**, *12*, 4398−4407.

(31) (a) Behr, J.-P.; Kirch, M.; Lehn, J.-M. Carrier-Mediated Transport through Bulk Liquid Membranes: Dependence of Transport Rates and Selectivity on Carrier Properties in a Diffusion-Limited Process. *J. Am. Chem. Soc.* **1985**, *107*, 241−246. (b) Vargas Jentzsch, A.; Emery, D.; Mareda, J.; Metrangolo, P.; Resnati, G.; Matile, S. Ditopic Ion Transport Systems: Anion-π Interactions and Halogen Bonds at Work. *Angew. Chem., Int. Ed.* **2011**, *50*, 11675−11678.

(32) Zhao, Y.; Cotelle, Y.; Sakai, N.; Matile, S. Unorthodox Interactions at Work. *J. Am. Chem. Soc.* **2016**, *138*, 4270−4277.

https://dx.doi.org/10.1021/jacs.9b13621
J. Am. Chem. Soc. 2020, 142, 4784−4792